J. Chem. Thermodynamics 128 (2019) 259–274

Contents lists available at ScienceDirect

J. Chem. Thermodynamics

journal homepage: www.elsevier.com/locate/jct

Thermal analysis and heat capacity study of polyethylene glycol (PEG) phase change materials for thermal energy storage applications

Yan Kou [a], Siyu Wang [a], Jipeng Luo [a,b], Keyan Sun [a,b], Jian Zhang [a], Zhicheng Tan [a,*], Quan Shi [a,*]

[a] Thermochemistry Laboratory, Dalian Institute of Chemical Physics, Chinese Academy of Science, Liaoning Province Key Laboratory of Thermochemistry for Energy and Materials, Dalian National Laboratory for Clean Energy, Dalian 116023, PR China
[b] University of Chinese Academy of Sciences, Beijing 100049, PR China

ARTICLE INFO

Article history:
Received 29 April 2018
Received in revised form 30 July 2018
Accepted 18 August 2018
Available online 23 August 2018

Keywords:
PEG
Phase change materials
Thermal energy storage
Heat capacity
Phase transition
Thermal conductivity

ABSTRACT

Phase change materials (PCMs) generally offer high latent heats for a wide range of thermal energy storage technologies. As typical organic PCMs, polyethylene glycol (PEG) has been widely studied due to their high latent enthalpy, non-toxic and non-corrosive natures. However, the thermal properties especially the heat capacities of PEG, which would play a vital role in theoretically and technically investigating PCM thermal performance, have never been studied in a wide temperature region. Herein, we reported the heat capacities of PEG samples with the molar massvarying from 1000 to 20,000 for the first time in the temperature range from (1.9 to 400) K using a combination method of Physical Property Measurement System (PPMS) and differential scanning calorimeter (DSC). Furthermore, the standard molar heat capacity, entropy and enthalpy at 298.15 K and 0.1 MPa were calculated based on the heat capacity curve fitting. Meanwhile, the phase transition temperature and enthalpy, thermal conductivity and thermal stability of these PEG samples were measured using various thermal analysis methods, and these thermal properties were also compared with the previous results.

1. Introduction

The energy crisis has become an increasing serious problem for the human society with the continuous consumption of energy resources on the earth, and consequently the development of energy storage technology has been always important for the effective utilization and rational management of non-renewable resources [1,2]. Recently, the technique of thermal energy storage using phase change materials (PCMs) has intrigued a great deal of interests due to the PCMs are capable of storing/releasing thermal energy during the phase transition process at almost constant temperatures with the involved latent heats absorbed/released. The density of thermal energy stored in PCMs is generally several times larger than that of commonly used sensible heat storage materials [3], and therefore PCMs based energy storage technique has potential applications in the field of industrial waste heat recovery, green building construction, solar energy utilization, heat management on electronic devices, intelligent temperature control clothing design, and so on [4–10].

As typical organic PCMs, polyethylene glycol (PEG) has been found to be a versatile PCM with high latent enthalpy, relatively wide transition temperature range and high thermal stability, ease of chemical modification, good biocompatibility and non-toxic and non-corrosive natures [11]. These remarkable properties have drawn much attention of researchers to synthesis new PCMs based on PEG and study their thermal performance. The popular methods of preparation of PEG based PCMs are physically blending PEG with other supporting materials, the chemical modification for achieving PEG solid–solid PCMs, and the vacuum impregnation in porous materials. For example, Yang et al. combined PEG6000, microcrystalline cellulose and graphene aerogels into a composite PCM, which showed a high latent heat of fusion of 156.1 $J{\cdot}g^{-1}$ and a thermal conductivity of 1.35 $W{\cdot}m^{-1}{\cdot}K^{-1}$ [12]. Zhou et al. synthesized a polyurethane-based solid–solid PCM using PEG, hexamethylene diisocyanate biuret and halloysite nanotubes, and the latent heat of the PCM could be improved to be 118.7 $J\,g^{-1}$ [13]. Wang et al. studied the crystallization behaviour of PEG confined in the mesoporous silica (SBA-15 and surface functional SBA), which confirmed the interactions between the PEG molecules and the channel surface of SBA-15 adjusted by the amino groups or methyl groups grafted on their internal surface [14].

Most studies on PEG-based PCMs mainly focus on the design and synthesis of new PCMs and improve their performance for thermal energy storage; however, their physically thermal properties with various molar masss, such as the thermal conductivity,

* Corresponding authors.
E-mail addresses: tzc@dicp.ac.cn (Z. Tan), shiquan@dicp.ac.cn (Q. Shi).

https://doi.org/10.1016/j.jct.2018.08.031
0021-9614/

phase transition property, heat capacity and the corresponding thermodynamic functions have seldom been investigated. Most importantly, the heat capacity is a fundamental thermodynamic property of a substance, and using the heat capacity data the related thermodynamic functions, such as entropy and enthalpy, can be derived based on the corresponding thermodynamic relationships. These thermodynamic properties are prerequisite for investigating the related thermal properties of PCMs for energy storage applications.

In this study, the thermal stability and thermal conductivity of some PEG samples with the average molar mass of 1000, 1500, 2000, 4000, 6000, 8000, 10000, 12,000 and 20,000 were measured using a thermal gravimetric and constants analyser, respectively. The phase transition properties of the PEG samples were investigated using a differential scanning calorimeter (DSC). The heat capacities of the PEG samples were measured in the temperature range from (1.9 to 400) K using a combination of Physical Property Measurement System and DSC, and the related thermodynamic functions were calculated based on the heat capacity curve fitting.

2. Experimental

The PEG1000, 2000, 4000, 6000, 10,000 and 20,000 samples were commercially provided by J&K Scientific Ltd. PEG1500, 8000 and 12,000 samples were provided by Alfa Aesar Chemical Co. Ltd. Before the calorimetric measurements, all of PEG samples were dried at 353 K in a vacuum oven for 48 h to remove the water absorbed on the sample surface. The detailed sample information of these PEG samples is listed in Table 1. The element analysis was performed using Flash smart organic elemental analyser (Thermo Fisher Scientific, USA), and the content of carbon, hydrogen and oxygen are listed in Table S1. The crystallization of PEG samples was verified using a powder X-ray diffraction technique with a Cu Karadiation (0.15418 nm) (PANalytical Co. X'pert PRO, Netherlands) operated under a voltage of 40 kV and a current of 40 mA. The thermal stability of PEG samples was assessed by a thermogravimetric analyser (TGA, SETSYS 16/18, SETARAM Co., France) from room temperature to 873 K with a heating rate of 10 K·min^{-1} under the high purity nitrogen atmosphere. The thermal conductivity measurement was performed on a thermal constants analyser (Hot Disk TPS2500S) at room temperature under atmospheric pressure for three times, and the averaged values were used as the samples' thermal conductivity.

The heat capacities of PEG samples were carried out using a Quantum Design PPMS from (1.9 to 300) K based on a relaxation calorimetric method. The standard uncertainty of heat capacity measurements using the PPMS was verified by measuring the heat capacities of a high purity copper pellet, α-Al_2O_3 (SRM720) and benzoic acid (SRM39j) to be within ± 3% in the temperature region from (1.9 to 20) K and ±1% from (20 to 300) K comparing the corresponding literature values [15]. The detailed sample preparation process and measurement procedure can be referred to the previous publications [16,17]. The heat capacity data were collected with a logarithmic temperature interval in temperature region from (1.9 to 100) K and a 10 K interval from (100 to 300) K. The sample amounts used in the measurements were 2.39 mg, 9.38 mg, 9.31 mg, 5.37 mg, 4.45 mg, 11.23 mg, 5.16 mg, 7.53 mg and 8.53 mg for PEG1000, PEG1500, PEG2000, PEG4000, PEG6000, PEG8000, PEG10000, PEG12000 and PEG20000, respectively.

The heat capacities of these PEG samples in the solid–liquid transition region were measured in the temperature range from (188 to 400) K, using a heat flux type differential scanning calorimeter (Discovery DSC from TA Instruments). The temperature calibration was performed by determining the melting temperature of indium. The extrapolated onset of indium was compared to the known melting point, and the difference was recorded for temperature calibration. The resultant calibration data curve, as a function of temperature, was sent to the instrument and applied to subsequent measurements. The DSC heat capacity measurement standard uncertainty was estimated to be within ±2% in the temperature range from (188 to 650) K with the heat capacity measurement of α-Al_2O_3 (SRM720). A benzoic acid sample (SRM 39j) from the US National Bureau of Standards was further measured using this DSC calorimeter, and the heat capacity measurement standard uncertainties was found to be ±5% in the temperature range from (188 to 300) K. The corresponding heat capacity measurement uncertainty plot was provided in the Supporting Information (Fig, S1). The powdered PEG samples were hermetically sealed in an aluminium pan (3.4 mL) and another empty aluminium pan was used as a reference. The sample amounts used in the measurements were 5.99 mg, 5.84 mg, 5.64 mg, 5.59 mg, 5.92 mg, 5.24 mg, 5.37 mg, 5.70 mg and 5.81 mg for PEG1000, PEG1500, PEG2000, PEG4000, PEG6000, PEG8000, PEG10000, PEG12000 and PEG20000, respectively. The temperature intervals in the measurement was set to be 1 K in non-transition region and 0.1 K in transition region with a heating rate of 10 K·min^{-1} and a high purity nitrogen purge gas flow rate of 50 mL·min^{-1}. In the DSC measurements, the samples were heated from 188 K to 400 K and held at 400 K for 10 min to erase the thermal history of the sample, following by cooling down to 188 K and then heated up to 400 K at the scanning rate of 10 K·min^{-1}, and the second run obtained in these DSC measurements were used in the heat capacity measurement and phase transition property determination for these PEG samples.

3. Results and discussion

3.1. XRD, TGA and thermal conductivity measurements

The XRD patterns of the PEG samples are shown in Fig. 1. Two characteristic diffraction peaks were observed at about 2θ = 19.2° and 23.4° for all PEG samples, which could be ascribed to the

Table 1
Sample information of PEG samples studied in this work.

Sample[a]	Source	Average molar mass	x_e/%[b]	w/%[c]
PEG1000	J&K Scientific Ltd.	1000	99.26	0.20
PEG1500	Alfa Aesar Chemical Co. Ltd.	1500	99.54	0.33
PEG2000	J&K Scientific Ltd.	2000	99.19	0.18
PEG4000	J&K Scientific Ltd.	4000	99.62	0.21
PEG6000	J&K Scientific Ltd.	6000	99.26	0.29
PEG8000	Alfa Aesar Chemical Co. Ltd.	8000	99.41	0.14
PEG10000	J&K Scientific Ltd.	10,000	99.34	0.17
PEG12000	Alfa Aesar Chemical Co. Ltd.	12,000	99.42	0.22
PEG20000	J&K Scientific Ltd.	20,000	99.36	0.21

[a] CAS number of PEG samples is 25322-68-3.
[b] The mass fraction purity was calculated using the method of elemental analysis.
[c] The water contents (mass fraction purity) of PEG after drying were measured by Karl Fisher analysis.

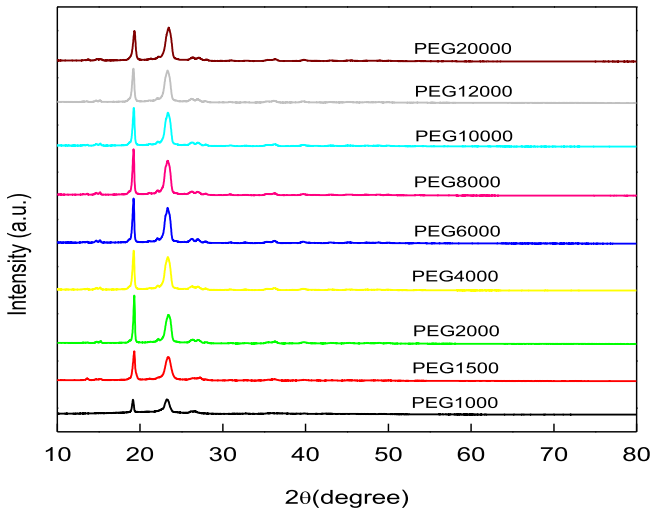

Fig. 1. XRD patterns of PEG samples.

PEG lattice plane of (1 2 0) and (1 3 2), respectively [13]. Also, the XRD diffraction peak intensity of these PEG samples decrease with their molar mass decreasing, indicating that the small molar mass samples may behave a higher segmental mobility and make their geometrical alignment more difficult than those of large molar mass samples [18]. Meanwhile, the intensity ratio between the two peaks increases gradually as the molar mass increasing, which is likely due to the PEG crystal thickness tends to increases as the average molar mass increasing [19]. This also may result in small phase transition enthalpies for small molar mass samples, which was confirmed in the following enthalpy determination using the DSC measurements.

The thermal stability of these PEG samples was investigated using the TGA technique, and the measured curves are shown in Fig. 2. It can be seen from the results that the PEG samples behave a thermal decomposition starting in the temperature region from (523 to 623) K and ending at temperatures above 723 K. Also, the decomposition starting temperatures of the large molar mass PEG samples are higher than those of small molar mass samples. These thermal behaviour for PEG are similar with those reported by Karaman et al. [20]. Based on these results, it can be concluded that all the PEG samples are thermally stable in the heat capacity measurement region below 400 K.

The thermal conductivity of the PEG samples measured using the thermal constants analyser is summarized in Table 2. It can be noted that the thermal conductivity increases with the molar mass increasing from 1000 to 6000, and then decreases with the molar mass continuously increasing to 20000. The largest thermal conductivity can be found to be 0.34 $W{\cdot}m^{-1}{\cdot}K^{-1}$ for PEG6000. The previous results for some PEG samples are also included in Table 2, and it can be seen that our measured thermal conductivities are in well agreement with these results.

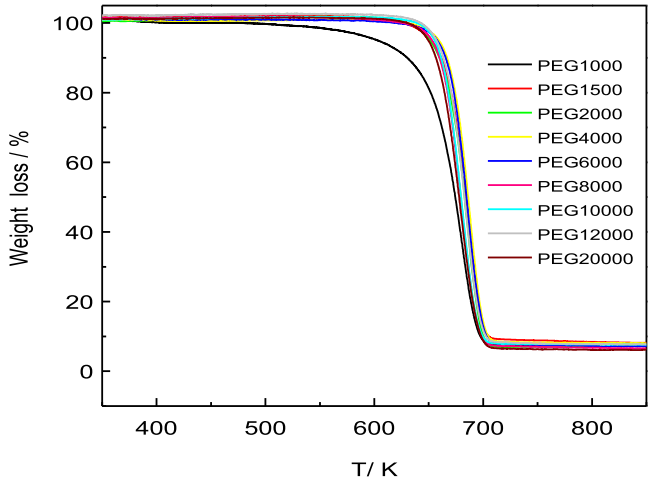

Fig. 2. TG curves of PEG samples.

3.2. Phase transition determination

The phase transition properties of the PEG samples, such as the melting/crystallization peak temperature (T_m/T_c) and transition enthalpy (H_m/H_c), were determined using the DSC technique in the temperature range from (188 to 400) K. These phase transition properties are extremely important to evaluate the thermal energy storage performance for PEG materials. The obtained DSC curves of the PEG samples are presented in Fig. 3, and the corresponding transition properties determined from the curve are listed in Table 3. As can be seen from the results, the melting/crystallization peak temperatures (T_m/T_c) generally increase with the sample molar mass increasing, while the transition enthalpies (H_m/H_c) firstly increase and then decrease with the maximum appearing in PEG10000. We also listed some previous results in Table 3 to make a comparison with ours. It can be seen the phase transition properties obtained in this work are roughly in agreement with the previous results, except that the PEG1000 crystallization peak temperature of 281.93 K is much lower than those reported from Karaman et al. [20] and Li et al. [24].

It should be noted that our DSC measurements on these PEG samples were started as low as 188 K, while the starting

Table 2
Thermal conductivity λ of PEG samples measured at temperature $T = 298$ K and pressure $p = 0.1$ MPa.[a]

Samples	λ/(W·m^{-1}·K^{-1}) This work				λ/(W·m^{-1}·K^{-1}) In Refs.
	Run 1	Run 2	Run 3	Average	
PEG1000	0.28	0.28	0.3	0.29	0.29 [20]
PEG1500	0.31	0.31	0.31	0.31	–
PEG2000	0.31	0.31	0.31	0.31	–
PEG4000	0.33	0.33	0.33	0.33	0.27 [21]
PEG6000	0.34	0.34	0.34	0.34	0.297 [22]
PEG8000	0.33	0.33	0.33	0.33	–
PEG10000	0.33	0.33	0.33	0.33	0.32 [23]
PEG12000	0.32	0.32	0.32	0.32	–
PEG20000	0.32	0.32	0.32	0.32	–

[a] The estimated standard uncertainties in the temperature T and pressure p are $u(T) = 0.1$ K, and $u(p) = 10$ kPa. The standard uncertainty of the thermal conductivity measurements is 0.05·λ.

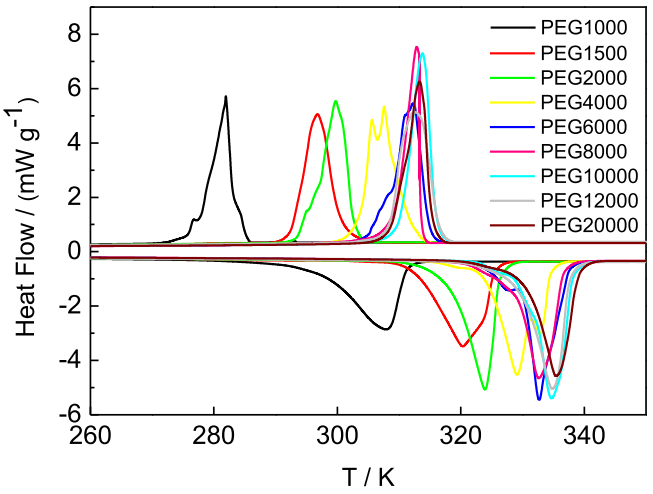

Fig. 3. DSC curves of PEG samples.

temperature is only 273.15 K and 183.15 K in the DSC measurements from Li and Karaman, respectively. To evaluate further the thermal history effect on the thermal properties of PEG1000, we performed DSC measurement again on PEG1000 at temperatures starting from 243.15 K. As can be seen from the results listed in Table 3, the crystallization peak temperature of PEG1000 in this run is roughly comparable with the literature results, even though the other thermal properties deviate a little from those obtained in the other run. This suggests that the thermal history is likely to greatly affect the transition properties of PEG samples, and we will further investigate this aspect in our future research.

3.3. Heat capacities

The experimental heat capacities of PEG samples measured using the PPMS in the temperature range from (1.9 to 300) K are listed in Table 4 and plotted against the temperature in Fig. 4. To better understand their heat capacity behaviour, we have used the average molar mass of these PEG samples to calculate their molar heat capacities. As can be seen from Fig. 4, the heat capacities of these PEG samples from the PPMS measurement increase with their average molar mass increasing. At temperatures above 160 K, the PEG heat capacities increase a little rapidly and behave a deviation from the normal heat capacity increasing trend. It may also note that the starting temperature of this thermal anomaly increase a little with the PEG molar mass increasing. This thermal anomaly is likely due to the PEG samples step into a glass transition or melting transition temperature region.

In order to calculate the thermodynamic functions, the experimental heat capacity data was fitted to a series of theoretical and empirical models in two temperature regions. In the low temperature region (T < 10 K), the heat capacities were fitted to the following theoretical model [15,34],

$$C^{o}_{p,m} = B_3T^3 + B_5T^5 + B_7T^7 + B_9T^9 \quad (1)$$

where the odd power terms in temperature represent the contribution from the lattice vibration, and this model may extrapolate the heat capacity to zero Kelvin to calculate the third law entropy. In the high temperature region above 10 K, the heat capacities of the PEG samples were fitted to the following orthogonal polynomial function [15,34],

$$C^{o}_{p,m} = A_0 + A_1T + A_2T^2 + A_3T^3 + A_4T^4 + A_5T^5 + A_6T^6 + A_7T^7 + A_8T^8 + A_9T^9 + A_{10}T^{10} \quad (2)$$

Table 3
Thermal properties of PEG samples obtained from DSC measurements obtained in this work and from previous results at pressure p = 0.1 MPa. The crystallization temperature and phase transition enthalpy are $T_{c,P}$ and ΔH_c, and the melting temperature and phase transition enthalpy are $T_{m,P}$ and ΔH_m.[a]

Sample	$T_{c,P}$ /K	ΔH_c/J·g^{-1}	ΔH_c/kJ·mol^{-1}	$T_{m,P}$/K	ΔH_m/(J·g^{-1})	ΔH_m/kJ·mol^{-1}	Sources
PEG1000	281.93	−144.38	−144.38	307.9	154.40	154.4	This work [b]
	296.15	−156.53	−156.53	310.22	161.18	161.18	This work [c]
	302.82	−166.71	−166.71	306.47	143.16	143.16	[20]
	300.65	−147.7	−147.7	310.05	156.1	156.1	[24]
PEG1500	296.78	−163.4	−245.1	320.38	161.43	242.15	This work
	295.85	−153.1	−229.65	323.25	160.5	240.75	[25]
	/	/	/	319.64	170.31	255.47	[26]
PEG2000	299.75	−161.48	−322.96	323.92	165.43	330.86	This work
	299.35	−139.7	−279.4	325.65	154.1	308.2	[21]
PEG4000	307.58	−171.31	−685.24	329.1	173.62	694.48	This work
	/	/	/	328.45	186.7	746.8	[27]
	305.45	−152.9	−611.6	335.95	164.9	659.6	[21]
	312.05	−181.4	−725.6	321.05	172.0	688	[28]
	311.65	−164.6	−658.4	333.66	180.3	721.2	[29]
PEG6000	312.27	−174.22	−1045.32	332.69	179.70	1078.20	This work
	312.75	−177.9	−1067.4	332.75	181.5	1089	[22]
	315.15	−172.7	−1036.2	324.05	174.7	1048.2	[28]
	310.75	−167.2	−1003.2	339.05	189.6	1137.6	[30]
PEG8000	312.86	−174.48	−1395.84	332.89	177.53	1420.24	This work
	322.05	−178.0	−1424	336.15	189.5	1516	[11]
PEG10000	313.79	−180.04	−1800.40	331.16	182.86	1828.6	This work
	319.85	−201.1	−2011	340.15	197.2	1972	[8]
	311.35	−154.0	−1540	334.65	162.4	1624	[31]
	323.25	−184	−1840	332.85	179	1790	[32]
PEG12000	312.55	−172.28	−2067.36	334.08	173.40	2080.80	This work
PEG20000	313.31	−164.72	−3294.40	335.42	168.50	3370.00	This work
	322.55	−154.2	−3084	334.35	176.2	3524	[33]

[a] The estimated standard uncertainties in the temperature T, pressure p, and transition enthalpy ΔH are $u(T)$ = 0.25 K, $u(p)$ = 0.05p, and $u(\Delta H)$ = 0.03ΔH.
[b] The first run DSC measurement. [c] The second run DSC measurement.

Table 4
Experimental molar heat capacities $C^{o}_{p,m}$ based on the average molar mass at constant pressure (p = 1.2 mPa) for PEG samples from T = (1.9 to 300) K.[a]

PEG1000		PEG1500		PEG2000	
T/(K)	$C_{p,m}$/(J·K^{-1}·mol^{-1})	T/(K)	$C_{p,m}$/(J·K^{-1}·mol^{-1})	T/(K)	$C_{p,m}$/(J·K^{-1}·mol^{-1})
1.917	0.21236	1.922	0.30487	1.918	0.39140
2.118	0.28834	2.119	0.40475	2.118	0.53005
2.341	0.39450	2.344	0.55076	2.341	0.68929
2.594	0.54093	2.597	0.75390	2.596	0.94883
2.874	0.74434	2.878	1.0377	2.878	1.3121
3.190	1.0333	3.195	1.4411	3.195	1.8235
3.534	1.4286	3.541	1.9962	3.540	2.5257
3.919	1.9618	3.927	2.7612	3.927	3.5056
4.346	2.7067	4.356	3.8334	4.355	4.8661
4.822	3.7218	4.834	5.3051	4.832	6.7389
5.352	5.0479	5.365	7.2581	5.363	9.2198
5.938	6.7875	5.954	9.8378	5.953	12.5176
6.592	8.9982	6.610	13.175	6.609	16.7779
7.321	11.8747	7.346	17.511	7.342	22.2584
8.128	15.5016	8.156	22.973	8.152	29.2206
9.024	19.8896	9.055	29.657	9.050	37.7211
10.093	25.732	10.116	38.474	10.115	48.9830
11.200	32.382	11.222	48.505	11.218	61.7158
12.433	40.426	12.446	60.201	12.433	77.6011
13.804	49.991	13.822	75.238	13.823	95.8716
15.350	61.076	15.354	92.743	15.346	117.88
17.022	74.666	17.044	113.00	17.037	143.50
18.905	90.142	18.921	136.44	18.915	173.46
21.003	107.87	21.000	163.13	20.980	208.60
23.323	127.63	23.330	193.04	23.304	245.83
25.897	149.60	25.876	226.41	25.867	288.58
28.716	174.29	28.729	263.96	28.718	336.77
31.882	201.17	31.900	304.15	31.890	388.34
35.405	230.85	35.416	348.39	35.413	444.83
39.318	262.98	39.333	395.63	39.287	507.03
43.632	296.03	43.650	444.93	43.629	571.27
48.424	329.00	48.454	496.42	48.424	637.25
53.738	365.65	53.784	551.47	53.749	708.08
59.656	405.45	59.704	610.26	59.676	783.94
66.223	445.88	66.275	671.69	66.249	863.68
73.529	486.43	73.589	734.36	73.550	945.08
81.616	530.99	81.686	803.36	81.649	1036.15
90.549	578.61	90.621	871.45	90.614	1122.57
100.525	615.72	100.564	937.41	100.575	1206.30
110.711	666.67	110.706	1009.43	110.725	1298.66
120.664	711.55	120.692	1074.05	120.733	1384.48
130.732	748.05	130.723	1133.86	130.771	1459.82
140.848	786.01	140.889	1190.46	140.909	1533.00
150.978	820.86	150.964	1245.34	151.002	1603.42
161.041	855.79	161.062	1297.56	161.115	1671.04
171.144	889.76	171.154	1350.01	171.204	1737.96
181.197	927.09	181.208	1404.18	181.255	1804.68
191.265	973.43	191.290	1458.89	191.318	1881.21
201.416	1008.61	201.423	1520.18	201.451	1948.53
211.517	1077.24	211.510	1608.95	211.556	2059.50
221.627	1149.83	221.599	1728.48	221.649	2213.90
231.722	1212.09	231.693	1825.30	231.759	2337.20
241.718	1271.80	241.699	1917.62	241.763	2458.62
251.796	1339.41	251.752	2018.37	251.825	2599.26
261.885	1408.42	261.835	2124.10	261.940	2740.99
271.941	1472.19	271.876	2239.58	272.000	2877.14
281.919	1588.03	281.861	2356.13	282.006	2988.86
		291.970	2473.58	292.146	3116.07

PEG4000		PEG6000		PEG8000	
T/(K)	$C_{p,m}$/(J·K^{-1}·mol^{-1})	T/(K)	$C_{p,m}$/(J·K^{-1}·mol^{-1})	T/(K)	$C_{p,m}$/(J·K^{-1}·mol^{-1})
1.920	0.76120	1.920	1.1479	1.922	1.4867
2.123	1.0242	2.125	1.5568	2.122	2.0212
2.350	1.3962	2.353	2.1347	2.346	2.7653
2.605	1.9305	2.609	2.9375	2.600	3.8077
2.894	2.6823	2.899	4.1087	2.883	5.2877
3.208	3.7330	3.214	5.6843	3.200	7.3924
3.556	5.1854	3.562	7.8833	3.547	10.314
3.943	7.2277	3.951	10.974	3.935	14.372
4.374	10.037	4.383	15.260	4.364	20.016
4.853	13.893	4.863	21.198	4.843	27.761
5.386	19.003	5.396	28.992	5.377	38.156

(*continued on next page*)

Table 4 (*continued*)

PEG4000		PEG6000		PEG8000	
T/(K)	$C_{p,m}$/(J·K^{-1}·mol^{-1})	T/(K)	$C_{p,m}$/(J·K^{-1}·mol^{-1})	T/(K)	$C_{p,m}$/(J·K^{-1}·mol^{-1})
5.976	25.749	5.988	39.259	5.968	51.819
6.632	34.419	6.645	52.505	6.626	69.319
7.365	45.673	7.377	69.566	7.359	92.012
8.178	59.793	8.190	91.019	8.170	120.43
9.078	77.046	9.093	117.49	9.067	155.50
10.129	99.465	10.144	151.46	10.128	200.36
11.234	125.24	11.241	190.41	11.231	253.09
12.465	156.50	12.473	238.32	12.472	316.20
13.829	194.52	13.838	294.95	13.834	392.92
15.371	238.03	15.374	361.95	15.360	482.43
17.056	290.06	17.067	441.34	17.046	587.25
18.944	350.71	18.945	534.59	18.934	708.32
21.032	419.58	21.038	638.08	21.019	846.98
23.357	496.53	23.359	756.24	23.324	1001.83
25.927	583.29	25.915	885.66	25.885	1179.80
28.762	679.57	28.771	1030.75	28.749	1368.80
31.935	782.74	31.933	1191.18	31.910	1578.65
35.459	896.54	35.459	1362.67	35.438	1808.95
39.361	1019.26	39.351	1548.25	39.314	2060.07
43.678	1146.99	43.665	1742.36	43.656	2317.06
48.480	1279.48	48.473	1941.61	48.445	2586.08
53.805	1422.62	53.800	2156.57	53.803	2870.88
59.724	1575.07	59.710	2386.33	59.705	3178.90
66.284	1734.58	66.268	2629.33	66.281	3497.12
73.598	1896.66	73.584	2871.00	73.591	3826.83
81.690	2078.80	81.679	3152.56	81.693	4194.20
90.656	2257.20	90.654	3415.90	90.663	4546.22
100.583	2423.09	100.591	3657.70	100.594	4884.23
110.788	2607.10	110.805	3944.88	110.759	5260.80
120.751	2777.30	120.759	4206.91	120.762	5611.54
130.784	2933.15	130.846	4433.14	130.837	5921.39
140.933	3080.91	140.932	4664.32	140.961	6211.33
151.031	3217.11	151.056	4869.96	151.032	6502.71
161.127	3355.69	161.167	5071.27	161.141	6777.84
171.228	3490.36	171.251	5274.57	171.249	7053.65
181.296	3624.80	181.330	5479.47	181.291	7319.36
191.384	3766.08	191.422	5656.83	191.363	7565.23
201.508	3882.44	201.506	5842.65	201.519	7815.27
211.619	4069.28	211.620	6080.86	211.614	8133.77
221.748	4300.83	221.730	6420.48	221.717	8526.75
231.833	4510.24	231.847	6763.46	231.800	8949.35
241.870	4693.13	241.853	7076.72	241.830	9361.33
251.950	4922.23	251.974	7430.56	251.910	9773.06
262.068	5185.90	262.039	7751.49	262.031	10243.05
272.128	5446.68	272.037	8127.04	272.098	10750.97
282.140	5759.75	282.090	8577.48	282.097	11283.00
292.279	5996.39	292.213	8966.24	292.212	11772.68
302.317	6255.21	302.291	9413.05	302.250	12391.00

PEG10000		PEG12000		PEG20000	
T/(K)	$C_{p,m}$/(J·K^{-1}·mol^{-1})	T/(K)	$C_{p,m}$/(J·K^{-1}·mol^{-1})	T/(K)	$C_{p,m}$/(J·K^{-1}·mol^{-1})
1.921	1.8612	1.922	2.2330	1.922	3.5766
2.126	2.5220	2.124	3.0406	2.124	4.8150
2.353	3.4522	2.350	4.1668	2.350	6.6309
2.606	4.7578	2.607	5.7756	2.603	9.1437
2.897	6.6705	2.896	8.0981	2.893	12.841
3.210	9.2975	3.210	11.259	3.205	17.795
3.559	12.937	3.558	15.717	3.553	24.958
3.947	18.058	3.946	21.931	3.941	34.936
4.378	25.122	4.377	30.666	4.370	48.728
4.857	34.842	4.856	42.584	4.850	67.748
5.392	47.787	5.389	58.491	5.383	93.127
5.983	64.771	5.980	79.465	5.972	126.54
6.639	86.755	6.639	106.49	6.631	169.71
7.373	114.90	7.373	141.54	7.363	225.48
8.186	150.60	8.184	184.77	8.173	295.71
9.087	194.18	9.084	238.96	9.076	381.25
10.137	250.37	10.134	308.69	10.129	493.27
11.244	315.59	11.240	388.45	11.237	621.16
12.479	394.34	12.460	486.36	12.467	776.56
13.851	488.27	13.843	602.12	13.840	962.19
15.386	598.86	15.370	740.47	15.366	1181.58
17.070	731.12	17.063	899.92	17.061	1438.95
18.964	883.58	18.943	1087.22	18.942	1740.07

Table 4 (*continued*)

PEG10000		PEG12000		PEG20000	
T/(K)	$C_{p,m}$/(J·K^{-1}·mol^{-1})	T/(K)	$C_{p,m}$/(J·K^{-1}·mol^{-1})	T/(K)	$C_{p,m}$/(J·K^{-1}·mol^{-1})
21.050	1055.20	21.021	1296.92	21.033	2077.70
23.379	1249.91	23.356	1537.67	23.352	2461.93
25.952	1466.25	25.905	1800.20	25.915	2886.66
28.789	1706.08	28.769	2091.58	28.752	3359.43
31.962	1966.15	31.936	2411.40	31.922	3871.41
35.493	2250.33	35.468	2761.59	35.441	4439.64
39.396	2555.24	39.329	3140.67	39.346	5037.30
43.720	2874.85	43.663	3533.74	43.685	5669.08
48.519	3201.09	48.465	3935.63	48.481	6320.53
53.856	3558.78	53.795	4363.57	53.799	7032.02
59.765	3937.08	59.718	4826.79	59.728	7776.70
66.334	4345.45	66.280	5313.80	66.298	8560.92
73.640	4753.84	73.594	5807.98	73.612	9363.69
81.748	5198.95	81.658	6394.16	81.705	10259.97
90.717	5640.62	90.665	6898.09	90.685	11111.02
100.645	6056.20	100.587	7414.33	100.609	11962.28
110.847	6532.93	110.754	7990.44	110.799	12867.70
120.815	6972.16	120.718	8521.85	120.749	13731.69
130.855	7347.92	130.760	8989.98	130.768	14484.01
140.974	7718.61	140.930	9441.29	140.919	15235.13
151.087	8072.50	151.025	9872.49	151.036	15915.91
161.145	8414.30	161.154	10301.42	161.159	16589.77
171.265	8762.29	171.194	10716.32	171.224	17284.22
181.310	9100.75	181.293	11141.12	181.291	17977.21
191.382	9437.79	191.372	11524.57	191.352	18574.62
201.522	9706.11	201.470	11872.27	201.509	19168.01
211.633	10084.87	211.643	12311.62	211.605	19904.34
221.748	10562.36	221.748	12905.81	221.707	20838.64
231.841	11048.75	231.839	13537.92	231.824	21823.66
241.857	11521.72	241.868	14148.55	241.812	22767.60
251.943	12033.10	251.944	14782.27	251.901	23752.00
262.070	12528.21	262.068	15377.75	262.014	24801.00
272.134	13124.23	272.143	16038.51	272.094	25839.92
282.124	13777.07	282.139	16799.06	282.077	26962.44
292.266	14455.36	292.263	17550.10	292.209	28180.16
302.311	15234.09	302.284	18496.64	302.239	29603.57

[a] The estimated standard uncertainties in the pressure p and temperature T are $u(p)$ = 0.10 mPa, and $u(T)$ = 0.01 K (2 < T/K < 20), $u(T)$ = 0.02 K (20 < T/K ⟨1 0 0), and $u(T)$ = 0.05 K (100 < T/K ⟨3 0 0). The standard uncertainties of the heat capacity measurements are 0.05·$C^{o}_{p,m}$ from T = (1.9 to 20) K and 0.02·$C^{o}_{p,m}$ from T = (20 to 300) K for all PEG samples except PEG1000. For PEG1000, the standard uncertainties of the heat capacity measurements are 0.1·$C^{o}_{p,m}$ from T = (1.9 to 20) K and 0.02·$C^{o}_{p,m}$ from T = (20 to 300) K.

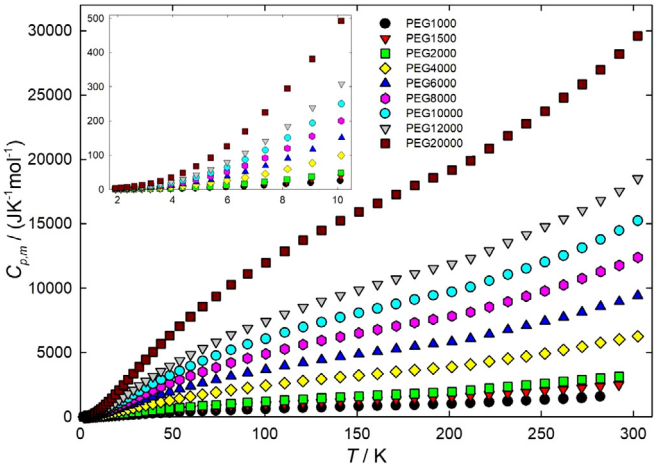

Fig. 4. Plot of the experimental heat capacities of PEG samples measured with PPMS.

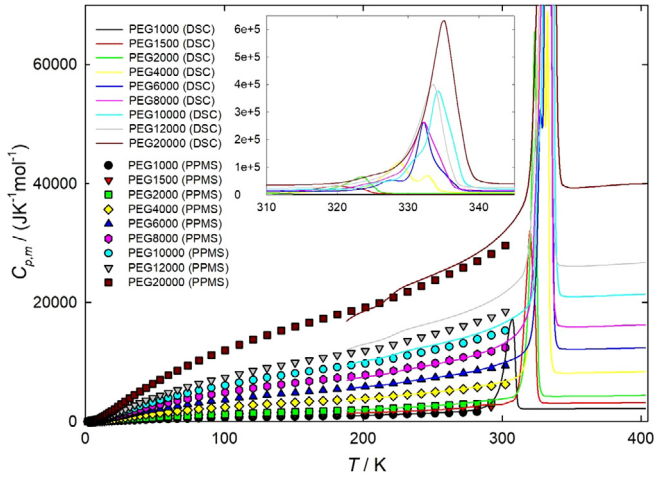

Fig. 5. Plot of the experimental heat capacities of PEG samples from DSC and PPMS measurements.

To further study the thermodynamic property at higher temperatures above 300 K, especially in the melting phase transition temperature region, the heat capacities of the PEG samples were measured using the DSC in the temperature range from 188 K up to 400 K. The measurement results are shown in Fig. 5 and the corresponding molar heat capacity data, calculated based on the average molar mass of the PEG samples, are presented in Supporting Information (SI). It can be seen in the heat capacity curve that all PEG samples behave a solid–liquid transition in this temperature region, which is in line with the heat flow curve in the DSC measurements.

Additionally, the heat capacities measured by PPMS were also shown in Fig. 5 to compare with the DSC data in the overlapping

temperature region. It can be noted that the DSC data of some PEG samples may deviate a little bit from the PPMS data. These slight deviations may be acceptable since two different calorimetric methods were employed, and most importantly, the DSC measurement uncertainties may be easily affected by sample amounts, morphologies, conductivities, and experimental conditions [33]. In order to calculate the thermodynamic function, we have scaled the DSC heat capacity data by multiplying a scaling factor to match the PPMS data to obtain smoothed heat capacities for the calculation in the entire temperature region [34]. The scaling factors are 1.050, 0.968, 1.044, 0.952, 0.913, and 1.033 for PEG1500, PEG2000, PEG8000, PEG10000, PEG12000 and PEG20000, respectively. The scaled DSC heat capacities in the solid and liquid phase temperature region were fitted to a polynomial function of equation (2), and the data in the melting transition region were fitted using a spline fitting method.

It should be pointed out that these PEG samples have a same monomer unit of (–C_2H_4O–), and consequently their molar heat capacities calculated using the molar mass of this monomer unit should be consistent with each other in the non-transition region. We have provided both PPMS and DSC heat capacity data based on the monomer unit in Table S2 and excel file, and plotted them as Figs. S2 and S3, respectively, in the Supporting Information. We selected PEG6000 as the reference sample since its average molar mass is in the middle of the average molar mass range of these PEG samples, and plotted the heat capacity deviations of the PEG samples from PEG6000 in Fig. S4 of the Supporting Information. It can be seen from the PPMS data that the deviations are roughly within ±5% in the temperature region below 10 K and within ±2% from (10 to 200) K, except that the PEG1000 deviation is within about ±10% below 10 K. In the temperature region above 200 K, the deviations of these PEG samples increase a lot since the solid–liquid transition gradually appears in these samples. As for the DSC data, we only provided the deviation plot in the liquid region due to the transition effect on the solid region. It can be seen that the deviations are roughly within ±5% for the PEG samples except PEG1000 and PEG12000, which agrees well with the DSC measurement uncertainties of the benzoic acid sample. As for the PEG1000 and PEG12000 samples, the deviations are roughly within ±7% and ±8%, respectively. Based on these deviations, we increased the heat capacity measurement uncertainties accordingly for these PEG samples.

All the fitting parameters and %RMS in the corresponding temperature regions are listed in Table 5 for PPMS data and Table 6 for DSC data. The small RMS% values indicate that these fits can be well representative of the measured heat capacity data. Based on these heat capacity fitting parameters, the thermodynamic functions of PEG samples have been calculated using the thermodynamic relationship of Eqs. (3) and (4) in the temperature range from (0 to 400) K, and the calculated results are listed in Table 7. The standard

Table 5
Fitting parameters in the fitting models for the experimental molar heat capacity of PEG samples measured by PPMS.

Parameters	PEG1000	PEG1500	PEG2000	PEG4000	PEG6000
Low T fits					
B_3/(J·mol^{-1}·K^{-4})	2.9432E−02	4.0933E−02	5.2396E−02	1.0192E−01	1.5453E−01
B_5/(J·mol^{-1}·K^{-6})	2.8702E−04	4.2293E−04	4.9830E−04	1.3580E−03	2.0356E−03
B_7/(J·mol^{-1}·K^{-8})	−6.8221E−06	−8.9197E−06	−1.0417E−05	−2.7813E−05	−4.1419E−05
B_9/(J·mol^{-1}·K^{-10})	3.5288E−08	4.3369E−08	4.9554E−08	1.3677E−07	2.0225E−07
%RMS	0.867	0.686	1.281	0.82	0.707
Rang/(K)	1.9 to 5.42	1.9 to 5.86	1.9 to 6.82	1.9 to 6.60	1.9 to 6.58
High T fits					
A_0/(J·mol^{-1}·K^{-1})	4.4889E+00	7.2817E+00	5.6602E+00	8.6235E+00	1.4074E+01
A_1/(J·mol^{-1}·K^{-2})	−2.9868E+00	−4.7379E+00	−4.6276E+00	−8.3383E+00	−1.3027E+01
A_2/(J·mol^{-1}·K^{-3})	6.7558E−01	1.0275E+00	1.1276E+00	2.1732E+00	3.3394E+00
A_3/(J·mol^{-1}·K^{-4})	−2.0054E−02	−2.9451E−02	−2.7831E−02	−5.2250E−02	−8.0799E−02
A_4/(J·mol^{-1}·K^{-5})	3.4542E−04	4.6775E−04	3.4961E−04	6.3383E−04	9.8612E−04
A_5/(J·mol^{-1}·K^{-6})	−3.8944E−06	−4.6202E−06	−2.4745E−06	−4.3164E−06	−6.7524E−06
A_6/(J·mol^{-1}·K^{-7})	2.9598E−08	2.9478E−08	9.8935E−09	1.6596E−08	2.6088E−08
A_7/(J·mol^{-1}·K^{-8})	−1.4994E−10	−1.2210E−10	−2.0762E−11	−3.3527E−11	−5.2941E−11
A_8/(J·mol^{-1}·K^{-9})	4.8264E−13	3.1854E−13	1.7743E−14	2.7632E−14	4.3817E−14
A_9/(J·mol^{-1}·K^{-10})	−8.8734E−16	−4.7699E−16			
A_{10}/(J·mol^{-1}·K^{-11})	7.0556E−19	3.1289E−19			
%RMS	0.323	0.373	0.757	0.948	0.873
Rang/(K)	5.42 to 201	5.86 to 269	6.82 to 201	6.60 to 252	6.58 to 202

Parameters	PEG8000	PEG10000	PEG12000	PEG20000
Low T fits				
B_3/(J·mol^{-1}·K^{-4})	1.9967E−01	2.4844E−01	2.9780E−01	4.7326E−01
B_5/(J·mol^{-1}·K^{-6})	3.0933E−03	3.8169E−03	5.0565E−03	8.1992E−03
B_7/(J·mol^{-1}·K^{-8})	−6.1922E−05	−7.6409E−05	−9.9518E−05	−1.6011E−04
B_9/(J·mol^{-1}·K^{-10})	3.0453E−07	3.7597E−07	4.9023E−07	7.8556E−07
%RMS	0.864	0.876	0.834	0.9
Rang/(K)	1.9 to 6.32	1.9 to 6.42	1.9 to 6.42	1.9 to 6.38
High T fits				
A_0/(J·mol^{-1}·K^{-1})	1.7927E+01	2.1415E+01	2.6781E+01	4.2435E+01
A_1/(J·mol^{-1}·K^{-2})	−1.7077E+01	−2.0976E+01	−2.6189E+01	−4.1698E+01
A_2/(J·mol^{-1}·K^{-3})	4.4183E+00	5.4733E+00	6.7949E+00	1.0834E+01
A_3/(J·mol^{-1}·K^{-4})	−1.0657E−01	−1.3216E−01	−1.6514E−01	−2.6195E−01
A_4/(J·mol^{-1}·K^{-5})	1.2960E−03	1.6081E−03	2.0208E−03	3.1918E−03
A_5/(J·mol^{-1}·K^{-6})	−8.8396E−06	−1.0973E−05	−1.3856E−05	−2.1812E−05
A_6/(J·mol^{-1}·K^{-7})	3.4025E−08	4.2265E−08	5.3588E−08	8.4134E−08
A_7/(J·mol^{-1}·K^{-8})	−6.8824E−11	−8.5595E−11	−1.0890E−10	−1.7060E−10
A_8/(J·mol^{-1}·K^{-9})	5.6811E−14	7.0792E−14	9.0308E−14	1.4121E−13
%RMS	0.876	0.925	0.936	0.884
Rang/(K)	6.32 to 202	6.42 to212	6.42 to 201	6.38 to 202

Table 6
Fitting parameters in solid–liquid transition region for the experimental molar heat capacity of PEG samples measured by DSC.

Parameters	PEG1000	PEG1500	PEG2000
Solid phase fits			
A_0/(J·mol^{-1}·K^{-1})	−2.149366301E+07	1.07663465373E+09	−2.148934713E+07
A_1/(J·mol^{-1}·K^{-2})	6.650359063E+05	−4.23335031011E+07	6.315279422E+05
A_2/(J·mol^{-1}·K^{-3})	−8.792792254E+03	7.37562014408E+05	−7.916106069E+03
A_3/(J·mol^{-1}·K^{-4})	6.439357068E+01	−7.47350812371E+03	5.486290304E+01
A_4/(J·mol^{-1}·K^{-5})	−2.820932665E−01	4.85372280980E+01	−2.270346405E−01
A_5/(J·mol^{-1}·K^{-6})	7.392042467E−04	−2.09536726016E−01	5.609698074E−04
A_6/(J·mol^{-1}·K^{-7})	−1.072823243E−06	6.01307582821E−04	−7.662899458E−07
A_7/(J·mol^{-1}·K^{-8})	6.652476024E−10	−1.10613286292E−06	4.464340192E−10
A_8/(J·mol^{-1}·K^{-9})		1.18361760675E−09	
A_9/(J·mol^{-1}·K^{-9})		−5.61340730417E−13	
%RMS	0.092	0.079	0.187
Rang/(K)	201 to 277	241 to 287	201 to 306
Liquid phase fits			
A_0/(J·mol^{-1}·K^{-1})	1.1801663E+04	5.56432330E+05	6.195966E+03
A_1/(J·mol^{-1}·K^{-2})	−8.0472952E+01	−5.95840851E+03	−1.330426E+01
A_2/(J·mol^{-1}·K^{-3})	2.1974701E−01	2.40303637E+01	2.097171E−02
A_3/(J·mol^{-1}·K^{-4})	−1.9643724E−04	−4.30180786E−02	
A_4/(J·mol^{-1}·K^{-5})		2.88501721E−05	
%RMS	0.098	0.105	0.041
Rang/(K)	316 to 400	330 to 405	336 to 410

Parameters	PEG4000	PEG6000	PEG8000
Solid phase fits			
A_0/(J·mol^{-1}·K^{-1})	−2.440008481E+07	−2.251423502E+07	−4.389715249E+07
A_1/(J·mol^{-1}·K^{-2})	6.983436073E+05	6.330083482E+05	1.257642691E+06
A_2/(J·mol^{-1}·K^{-3})	−8.521198285E+03	−7.581301547E+03	−1.536407688E+04
A_3/(J·mol^{-1}·K^{-4})	5.747069758E+01	5.014937993E+01	1.037732940E+02
A_4/(J·mol^{-1}·K^{-5})	−2.313934136E−01	−1.978947078E−01	−4.185794855E−01
A_5/(J·mol^{-1}·K^{-6})	5.562346384E−04	4.659301871E−04	1.008490476E−03
A_6/(J·mol^{-1}·K^{-7})	−7.392643798E−07	−6.061691023E−07	−1.344150143E−06
A_7/(J·mol^{-1}·K^{-8})	4.191261343E−10	3.362571671E−10	7.647612052E−10
%RMS	0.081	0.088	0.153
Rang/(K)	252 to 306	201 to310	202 to 307
Liquid phase fits			
A_0/(J·mol^{-1}·K^{-1})	1.14725669E+05	1.80938363E+05	2.54640264E+05
A_1/(J·mol^{-1}·K^{-2})	−8.54004419E+02	−1.33711468E+03	−1.88849414E+03
A_2/(J·mol^{-1}·K^{-3})	2.26861854E+00	3.51402349E+00	4.97067717E+00
A_3/(J·mol^{-1}·K^{-4})	−1.99584467E−03	−3.06203579E−03	−4.33768220E−03
%RMS	0.108	0.089	0.068
Rang/(K)	340 to 410	343 to 410	344 to 410

Parameters	PEG10000	PEG12000	PEG20000
Solid phase fits			
A_0/(J·mol^{-1}·K^{-1})	8.6301239383E+08	1.774562648948E+10	3.138541530054E+10
A_1/(J·mol^{-1}·K^{-2})	−3.3020327461E+07	−7.322215871347E+08	−1.308350194395E+09
A_2/(J·mol^{-1}·K^{-3})	5.5800969654E+05	1.354131674767E+07	2.443567698211E+07
A_3/(J·mol^{-1}·K^{-4})	−5.4672637423E+03	−1.478104333476E+05	−2.692720034897E+05
A_4/(J·mol^{-1}·K^{-5})	3.4232509299E+01	1.054646050762E+03	1.938919352220E+03
A_5/(J·mol^{-1}·K^{-6})	−1.4207459042E−01	−5.139978553498E+00	−9.532992550030E+00
A_6/(J·mol^{-1}·K^{-7})	3.9091050914E−04	1.732955774024E−02	3.241322499474E−02
A_7/(J·mol^{-1}·K^{-8})	−6.8770354063E−07	−3.991329946867E−05	−7.526187267979E−05
A_8/(J·mol^{-1}·K^{-9})	7.0204292729E−10	6.010443531906E−08	1.142210884451E−07
A_9/(J·mol^{-1}·K^{-9})	−3.1691073871E−13	−5.344059425486E−11	−1.023192003901E−10
A_{10}/(J·mol^{-1}·K^{-9})		2.130589048447E−14	4.108650906223E−14
%RMS	0.1	0.081	0.164
Rang/(K)	212 to 310	201 to 310	202 to 310
Liquid phase fits			
A_0/(J·mol^{-1}·K^{-1})	2.4781845E+04	3.4909810E+04	1.3434719E+04
A_1/(J·mol^{-1}·K^{-2})	−3.3071553E+01	−6.8935558E+01	1.3043157E+02
A_2/(J·mol^{-1}·K^{-3})	5.5018661E−02	1.0638516E−01	−1.5206218E−01
A_3/(J·mol^{-1}·K^{-4})			
%RMS	0.07	0.063	0.06
Rang/(K)	347 to 410	347 to 410	351 to 410

molar heat capacity ($C^o_{p,m}$), entropy (S^o_m) and enthalpy (H^o_m) at 298.15 K and 0.1 MPa have been determined to be (5767.85 ± 115.36) J·K^{-1}·mol^{-1}, (1753.06 ± 35.06) J·K^{-1}·mol^{-1} and (276.56 ± 5.54) kJ·mol^{-1} for PEG1000; (2992.37 ± 59.44) J·K^{-1}·mol^{-1}, (2735.50 ± 54.75) J·K^{-1}·mol^{-1} and (436.54 ± 8.74) kJ·mol^{-1} for PEG1500; (3612.71 ± 72.26) J·K^{-1}·mol^{-1}, (3195.74 ± 63.92) J·K^{-1}·mol^{-1} and (478.75 ± 9.58) kJ·mol^{-1} for PEG2000; (6564.54 ± 131.3) J·K^{-1}·mol^{-1}, (6306.98 ± 126.08) J·K^{-1}·mol^{-1} and (930.98 ± 18.62) kJ·mol^{-1} for PEG4000; (9633.64 ± 192.68) J·K^{-1}·mol^{-1}, (9488.32 ± 189.76) J·K^{-1}·mol^{-1} and (1394.12 ± 27.88) kJ·mol^{-1} for PEG6000; (13281.44 ± 265.62) J·K^{-1}·mol^{-1}, (12726.68 ± 254.54) J·K^{-1}·mol^{-1} and (1879.33 ± 37.58)

Table 7
Standard thermodynamic functions of PEG samples as a function of temperature T at the standard pressure p^o = 0.1 MPa.[a]

PEG1000				PEG1500			
T/K	$C^o_{p,m}$/ (J·K^{-1}·mol^{-1})	$\Delta^T_0 S^o_m$/ (J·K^{-1}·mol^{-1})	$\Delta^T_0 H^o_m$/ (kJ·mol^{-1})	T/K	$C^o_{p,m}$/ (J·K^{-1}·mol^{-1})	$\Delta^T_0 S^o_m$/ (J·K^{-1}·mol^{-1})	$\Delta^T_0 H^o_m$/ (kJ·mol^{-1})
Solid region				Solid region			
0	0	0	0	0	0	0	0
1	2.9712E−02	9.8670E−03	7.4049E−06	1	4.1347E−02	1.3728E−02	1.0303E−05
2	2.4378E−01	8.0198E−02	1.2057E−04	2	3.3988E−01	1.1170E−01	1.6796E−04
3	8.5017E−01	2.7678E−01	6.2548E−04	3	1.1893E+00	3.8626E−01	8.7321E−04
4	2.0750E+00	6.7172E−01	2.0274E−03	4	2.9180E+00	9.4023E−01	2.8399E−03
5	4.1118E+00	1.3372E+00	5.0475E−03	5	5.8261E+00	1.8797E+00	7.1039E−03
6	6.9758E+00	2.3293E+00	1.0533E−02	6	1.0055E+01	3.2966E+00	1.4939E−02
7	1.0573E+01	3.6655E+00	1.9247E−02	7	1.5412E+01	5.2344E+00	2.7579E−02
8	1.4858E+01	5.3498E+00	3.1908E−02	8	2.1832E+01	7.7003E+00	4.6117E−02
9	1.9761E+01	7.3772E+00	4.9169E−02	9	2.9210E+01	1.0689E+01	7.1563E−02
10	2.5217E+01	9.7371E+00	7.1615E−02	10	3.7446E+01	1.4186E+01	1.0482E−01
15	5.8851E+01	2.6013E+01	2.7798E−01	15	8.8493E+01	3.8542E+01	4.1377E−01
20	9.9068E+01	4.8347E+01	6.7098E−01	20	149.71	7.2226E+01	1.0065E+00
25	141.98	7.5040E+01	1.2731E+00	25	214.95	112.61	1.9175E+00
30	185.19	104.75	2.0913E+00	30	280.35	157.60	3.1562E+00
35	227.29	136.48	3.1231E+00	35	343.71	205.61	4.7175E+00
40	267.55	169.48	4.3610E+00	40	403.94	255.47	6.5880E+00
45	305.70	203.22	5.7951E+00	45	460.72	306.36	8.7511E+00
50	341.68	237.31	7.4144E+00	50	514.15	357.70	1.1190E+01
55	375.63	271.48	9.2085E+00	55	564.56	409.09	1.3888E+01
60	407.71	305.56	1.1168E+01	60	612.41	460.28	1.6831E+01
65	438.12	339.40	1.3283E+01	65	658.11	511.11	2.0008E+01
70	467.08	372.94	1.5546E+01	70	702.06	561.50	2.3409E+01
75	494.76	406.11	1.7951E+01	75	744.52	611.40	2.7026E+01
80	521.33	438.90	2.0492E+01	80	785.71	660.77	3.0852E+01
85	546.92	471.28	2.3163E+01	85	825.72	709.61	3.4881E+01
90	571.66	503.24	2.5960E+01	90	864.60	757.91	3.9108E+01
95	595.64	534.79	2.8878E+01	95	902.33	805.67	4.3525E+01
100	618.93	565.94	3.1915E+01	100	938.87	852.89	4.8129E+01
110	663.64	627.05	3.8330E+01	110	1008.14	945.67	5.7868E+01
120	706.00	686.63	4.5180E+01	120	1072.10	1036.17	6.8274E+01
130	745.98	744.73	5.2442E+01	130	1130.91	1124.34	7.9293E+01
140	783.49	801.40	6.0091E+01	140	1185.36	1210.16	9.0878E+01
150	818.65	856.67	6.8104E+01	150	1236.86	1293.71	102.99
160	852.16	910.58	7.6459E+01	160	1287.36	1375.15	115.61
170	885.55	963.24	8.5147E+01	170	1339.12	1454.73	128.74
180	921.22	1014.85	9.4177E+01	180	1394.56	1532.82	142.41
190	962.08	1065.72	103.59	190	1456.02	1609.84	156.65
200	1010.72	1116.27	113.45	200	1525.58	1686.25	171.55
210	1081.96	1167.23	123.89	210	1604.77	1762.56	187.20
220	1155.31	1219.27	135.08	220	1694.21	1839.24	203.68
230	1226.79	1272.19	146.99	230	1793.17	1916.70	221.11
240	1310.20	1326.09	159.66	240	1899.30	1995.24	239.57
250	1418.78	1381.69	173.28	250	2011.98	2297.04	315.85
260	1548.61	1439.82	188.11	260	2148.25	2378.50	336.62
270	1694.12	1500.91	204.30	270	2337.68	2462.86	358.98
273.15	1750.21	1520.88	209.72	273.15	2420.43	2490.44	366.47
Melting region				280	2655.85	2553.14	383.81
280	1949.56	1566.30	222.29	Melting region			
290	2736.61	1646.24	245.09	290	2974.20	2652.72	412.20
298.15	5767.85	1753.06	276.56	298.15	2992.37	2735.50	436.54
300	7552.28	1793.90	288.77	300	3033.12	2754.11	442.11
305	15410.45	1979.59	345.00	305	3438.04	2807.24	458.18
310	7294.33	2224.78	420.35	310	4428.08	2867.63	476.76
315	2134.22	2272.30	435.17	315	14507.40	2998.70	517.78
Liquid region				320	33739.51	3386.01	640.88
320	2115.56	2305.68	445.77	325	8500.75	3760.61	761.54
325	2115.41	2338.47	456.35	330	3277.21	3823.94	782.26
330	2116.67	2370.78	466.93	Liquid region			
335	2119.20	2402.63	477.52	335	3244.32	3872.86	798.53
340	2122.84	2434.05	488.12	340	3236.16	3920.85	814.72
345	2127.46	2465.07	498.75	345	3236.15	3968.09	830.90
350	2132.89	2495.72	509.40	350	3241.68	4014.69	847.09
355	2139.00	2526.02	520.08	355	3250.56	4060.73	863.32
360	2145.64	2555.98	530.79	360	3261.04	4106.27	879.60
365	2152.65	2585.62	541.53	365	3271.79	4151.32	895.93
370	2159.90	2614.96	552.31	370	3281.92	4195.90	912.32
375	2167.23	2644.00	563.13	375	3290.97	4240.02	928.75
380	2174.50	2672.76	573.99	380	3298.94	4283.66	945.23
385	2181.57	2701.23	584.88	385	3306.21	4326.83	961.74

Table 7 (*continued*)

PEG1000				PEG1500			
T/K	$C^o_{p,m}$/ (J·K^{-1}·mol^{-1})	$\Delta^T_0 S^o_m$/ (J·K^{-1}·mol^{-1})	$\Delta^T_0 H^o_m$/ (kJ·mol^{-1})	T/K	$C^o_{p,m}$/ (J·K^{-1}·mol^{-1})	$\Delta^T_0 S^o_m$/ (J·K^{-1}·mol^{-1})	$\Delta^T_0 H^o_m$/ (kJ·mol^{-1})
390	2188.27	2729.42	595.80	390	3313.64	4369.54	978.29
395	2194.47	2757.34	606.76	395	3322.50	4411.81	994.88
400.00	2200.02	2784.98	617.74	400.00	3334.50	4453.67	1011.52
PEG2000				PEG4000			
T/K	$C^o_{p,m}$/ (J·K^{-1}·mol^{-1})	$\Delta^T_0 S^o_m$/ (J·K^{-1}·mol^{-1})	$\Delta^T_0 H^o_m$/ (kJ·mol^{-1})	T/K	$C^o_{p,m}$/ (J·K^{-1}·mol^{-1})	$\Delta^T_0 S^o_m$/ (J·K^{-1}·mol^{-1})	$\Delta^T_0 H^o_m$/ (kJ·mol^{-1})
Solid region				Solid region			
0	0	0	0	0	0	0	0
1	5.2884E−02	1.7563E−02	1.3181E−05	1	1.0325E−01	3.4242E−02	2.5704E−05
2	4.3380E−01	1.4272E−01	2.1457E−04	2	8.5535E−01	2.7999E−01	4.2130E−04
3	1.5140E+00	4.9263E−01	1.1133E−03	3	3.0238E+00	9.7492E−01	2.2069E−03
4	3.7059E+00	1.1969E+00	3.6134E−03	4	7.4938E+00	2.3914E+00	7.2367E−03
5	7.3896E+00	2.3891E+00	9.0242E−03	5	1.5078E+01	4.8148E+00	1.8237E−02
6	1.2776E+01	4.1863E+00	1.8964E−02	6	2.6168E+01	8.4913E+00	3.8570E−02
7	1.9770E+01	6.6626E+00	3.5118E−02	7	4.0273E+01	1.3555E+01	7.1602E−02
8	2.7906E+01	9.8201E+00	5.8854E−02	8	5.6710E+01	1.9979E+01	1.1989E−01
9	3.7207E+01	1.3633E+01	9.1318E−02	9	7.5432E+01	2.7718E+01	1.8578E−01
10	4.7566E+01	1.8081E+01	1.3362E−01	10	9.6235E+01	3.6725E+01	2.7145E−01
15	111.94	4.8918E+01	5.2472E−01	15	225.17	9.8888E+01	1.0597E+00
20	190.11	9.1598E+01	1.2759E+00	20	381.76	184.65	2.5690E+00
25	274.53	143.03	2.4361E+00	25	551.31	287.92	4.8987E+00
30	360.02	200.65	4.0228E+00	30	723.51	403.67	8.0863E+00
35	443.26	262.44	6.0325E+00	35	891.59	527.91	1.2127E+01
40	522.33	326.85	8.4485E+00	40	1051.49	657.51	1.6988E+01
45	596.35	392.69	1.1247E+01	45	1201.21	790.10	2.2625E+01
50	665.18	459.13	1.4403E+01	50	1340.23	923.95	2.8983E+01
55	729.19	525.57	1.7891E+01	55	1469.07	1057.81	3.6010E+01
60	789.04	591.61	2.1688E+01	60	1588.92	1190.83	4.3658E+01
65	845.50	657.01	2.5776E+01	65	1701.30	1322.50	5.1887E+01
70	899.37	721.66	3.0139E+01	70	1807.82	1452.51	6.0662E+01
75	951.39	785.49	3.4766E+01	75	1910.05	1580.74	6.9958E+01
80	1002.16	848.52	3.9651E+01	80	2009.37	1707.19	7.9757E+01
85	1052.12	910.78	4.4787E+01	85	2106.87	1831.94	9.0048E+01
90	1101.56	972.31	5.0171E+01	90	2203.35	1955.10	100.82
95	1150.57	1033.19	5.5802E+01	95	2299.27	2076.80	112.08
100	1199.13	1093.44	6.1676E+01	100	2394.80	2197.17	123.82
110	1294.08	1212.21	7.4145E+01	110	2583.99	2434.32	148.71
120	1384.25	1328.72	8.7542E+01	120	2767.68	2667.09	175.48
130	1467.17	1442.85	101.81	130	2941.03	2895.55	204.03
140	1541.28	1554.35	116.86	140	3099.61	3119.41	234.25
150	1606.70	1662.96	132.60	150	3241.20	3338.19	265.97
160	1665.71	1768.56	148.97	160	3366.93	3551.46	299.02
170	1722.68	1871.25	165.91	170	3481.69	3759.06	333.27
180	1783.49	1971.41	183.43	180	3593.78	3961.23	368.64
190	1854.53	2069.68	201.61	190	3713.59	4158.69	405.17
200	1941.36	2166.93	220.58	200	3851.82	4352.58	442.98
210	2039.75	2263.83	240.44	210	4017.19	4544.39	482.30
220	2167.16	2361.61	261.46	220	4214.12	4735.69	523.43
230	2296.41	2460.82	283.79	230	4441.01	4927.92	566.68
240	2416.80	2561.12	307.36	240	4689.37	5122.12	612.32
250	2545.84	2662.31	332.15	250	4944.94	5318.74	660.49
260	2712.80	2765.25	358.40	260	5138.42	5515.87	710.76
270	2930.64	2871.57	386.58	270	5419.88	5714.89	763.50
273.15	3007.35	2906.01	395.93	273.15	5522.07	5778.34	780.73
280	3178.57	2982.60	417.12	280	5768.03	5918.08	819.38
290	3418.06	3098.38	450.12	290	6180.48	6127.51	879.08
298.15	3612.71	3195.74	478.75	298.15	6564.54	6303.98	930.98
300	3664.47	3218.24	485.48	300	6660.62	6344.88	943.21
305	3844.75	3280.20	504.23	305	6948.95	6457.28	977.21
Melting region				Melting region			
310	4414.22	3345.38	524.27	310	7377.69	6573.35	1012.91
315	8300.96	3438.76	553.48	315	8736.02	6699.65	1052.38
320	27563.40	3680.76	630.43	320	14055.10	6877.18	1108.78
325	31798.84	4412.49	866.55	325	39337.03	7195.06	1211.45
330	4189.64	4543.48	909.33	330	79791.51	8483.50	1633.87
335	4102.20	4605.49	929.95	335	12445.95	9228.96	1881.43
Liquid region				Liquid region			
340	4096.85	4666.18	950.43	340	8192.15	9362.10	1926.34
345	4102.15	4726.02	970.93	345	8159.85	9481.30	1967.17

(*continued on next page*)

Table 7 (*continued*)

PEG2000				PEG4000			
T/K	$C^o_{p,m}$/ (J·K^{-1}·mol^{-1})	$\Delta^T_0 S^o_m$/ (J·K^{-1}·mol^{-1})	$\Delta^T_0 H^o_m$/ (kJ·mol^{-1})	T/K	$C^o_{p,m}$/ (J·K^{-1}·mol^{-1})	$\Delta^T_0 S^o_m$/ (J·K^{-1}·mol^{-1})	$\Delta^T_0 H^o_m$/ (kJ·mol^{-1})
350	4108.51	4785.09	991.45	350	8158.05	9598.68	2007.96
355	4115.91	4843.42	1012.02	355	8164.91	9714.44	2048.76
360	4124.37	4901.05	1032.62	360	8178.91	9828.73	2089.62
365	4133.87	4958.00	1053.26	365	8198.57	9941.67	2130.56
370	4144.42	5014.31	1073.96	370	8222.39	10053.38	2171.61
375	4156.01	5070.02	1094.71	375	8248.87	10163.92	2212.79
380	4168.66	5125.15	1115.52	380	8276.52	10273.36	2254.10
385	4182.36	5179.73	1136.40	385	8303.83	10381.73	2295.55
390	4197.10	5233.79	1157.34	390	8329.32	10489.05	2337.14
395	4212.89	5287.36	1178.37	395	8351.47	10595.30	2378.84
400	4229.73	5340.46	1199.47	400	8368.81	10700.47	2420.64
PEG6000				PEG8000			
T/K	$C^o_{p,m}$/ (J·K^{-1}·mol^{-1})	$\Delta^T_0 S^o_m$/ (J·K^{-1}·mol^{-1})	$\Delta^T_0 H^o_m$/ (kJ·mol^{-1})	T/K	$C^o_{p,m}$/ (J·K^{-1}·mol^{-1})	$\Delta^T_0 S^o_m$/ (J·K^{-1}·mol^{-1})	$\Delta^T_0 H^o_m$/ (kJ·mol^{-1})
Solid region				Solid region			
0	0	0	0	0	0	0	0
1	1.5653E−01	5.1912E−02	3.8967E−05	1	2.0270E−01	6.7166E−02	5.0425E−05
2	1.2962E+00	4.2437E−01	6.3853E−04	2	1.6886E+00	5.5113E−01	8.2972E−04
3	4.5804E+00	1.4772E+00	3.3438E−03	3	6.0133E+00	1.9287E+00	4.3702E−03
4	1.1349E+01	3.6225E+00	1.0962E−02	4	1.5012E+01	4.7571E+00	1.4415E−02
5	2.2837E+01	7.2927E+00	2.7622E−02	5	3.0382E+01	9.6279E+00	3.6528E−02
6	3.9651E+01	1.2862E+01	5.8424E−02	6	5.2917E+01	1.7052E+01	7.7587E−02
7	6.1057E+01	2.0538E+01	1.0849E−01	7	8.1296E+01	2.7282E+01	1.4432E−01
8	8.6034E+01	3.0281E+01	1.8173E−01	8	114.54	4.0254E+01	2.4183E−01
9	114.50	4.2025E+01	2.8172E−01	9	152.42	5.5889E+01	3.7495E−01
10	146.16	5.5701E+01	4.1180E−01	10	194.52	7.4092E+01	5.4808E−01
15	342.42	150.19	1.6100E+00	15	455.47	199.80	2.1422E+00
20	580.68	280.62	3.9055E+00	20	772.27	373.28	5.1953E+00
25	838.36	437.69	7.4488E+00	25	1115.03	582.17	9.9076E+00
30	1099.73	613.68	1.2295E+01	30	1462.86	816.25	1.6354E+01
35	1354.46	802.46	1.8435E+01	35	1802.04	1067.40	2.4522E+01
40	1596.42	999.28	2.5818E+01	40	2124.38	1329.28	3.4346E+01
45	1822.66	1200.54	3.4373E+01	45	2425.90	1597.12	4.5730E+01
50	2032.51	1403.58	4.4017E+01	50	2705.66	1867.38	5.8568E+01
55	2226.85	1606.53	5.4672E+01	55	2964.79	2137.57	7.2753E+01
60	2407.57	1808.13	6.6263E+01	60	3205.76	2405.99	8.8186E+01
65	2577.04	2007.59	7.8729E+01	65	3431.71	2671.60	104.79
70	2737.79	2204.50	9.2019E+01	70	3646.00	2933.82	122.48
75	2892.23	2398.69	106.10	75	3851.84	3192.43	141.23
80	3042.45	2590.16	120.93	80	4052.04	3447.44	160.99
85	3190.10	2779.05	136.52	85	4248.85	3699.01	181.75
90	3336.36	2965.53	152.83	90	4443.86	3947.39	203.48
95	3481.87	3149.82	169.88	95	4638.01	4192.86	226.18
100	3626.82	3332.11	187.65	100	4831.58	4435.69	249.86
110	3913.72	3691.28	225.36	110	5215.45	4914.24	300.10
120	4191.56	4043.82	265.90	120	5588.45	5384.15	354.13
130	4452.49	4389.77	309.13	130	5940.21	5845.53	411.80
140	4689.53	4728.57	354.87	140	6261.20	6297.71	472.83
150	4899.26	5059.43	402.83	150	6546.26	6739.61	536.90
160	5083.62	5381.62	452.76	160	6797.11	7170.27	603.64
170	5250.54	5694.88	504.45	170	7023.16	7589.22	672.76
180	5413.11	5999.58	557.76	180	7240.65	7996.80	744.08
190	5587.70	6296.84	612.75	190	7470.20	8394.33	817.61
200	5790.86	6588.46	669.61	200	7733.04	8784.00	893.59
210	6031.84	6877.05	728.77	210	8107.12	9170.74	972.87
220	6312.33	7163.85	790.43	220	8539.20	9557.46	1056.02
230	6647.16	7451.71	855.20	230	9033.41	9947.88	1143.87
240	6990.46	7741.90	923.40	240	9515.39	10342.65	1236.64
250	7318.15	8033.96	994.95	250	9962.31	10740.23	1334.05
260	7645.86	8327.31	1069.76	260	10412.74	11139.62	1435.89
270	8017.16	8622.61	1148.02	270	10933.71	11542.04	1542.54
273.15	8150.99	8716.37	1173.48	273.15	11122.35	11669.94	1577.28
280	8478.92	8922.19	1230.40	280	11583.70	11950.96	1655.00
290	9061.00	9229.50	1318.00	290	12409.87	12371.25	1774.80
298.15	9633.64	9488.32	1394.12	298.15	13281.44	12726.68	1879.33
300	9777.00	9548.35	1412.07	300	13518.28	12809.56	1904.11
305	10193.54	9713.33	1461.98	305	14269.35	13038.94	1973.51
310	10663.12	9882.81	1514.09	Melting region			
Melting region				310	15242.54	13278.48	2047.17
315	11484.47	10059.53	1569.32	315	16941.29	13534.74	2127.26

Table 7 (*continued*)

PEG6000				PEG8000			
T/K	$C^o_{p,m}$/ (J·K^{-1}·mol^{-1})	$\Delta_0^T S^o_m$/ (J·K^{-1}·mol^{-1})	$\Delta_0^T H^o_m$/ (kJ·mol^{-1})	T/K	$C^o_{p,m}$/ (J·K^{-1}·mol^{-1})	$\Delta_0^T S^o_m$/ (J·K^{-1}·mol^{-1})	$\Delta_0^T H^o_m$/ (kJ·mol^{-1})
320	13678.45	10253.47	1630.91	320	20982.40	13825.35	2219.55
325	29046.23	10546.45	1725.49	325	46006.38	14316.73	2378.19
330	63740.13	11263.39	1960.43	330	128437.39	15427.99	2742.57
335	82215.57	13557.69	2723.16	335	109423.97	18454.52	3748.64
340	12569.80	14017.85	2878.04	340	16937.99	18955.43	3917.26
Liquid region				Liquid region			
345	12152.15	14196.58	2939.25	345	16623.68	19199.72	4000.93
350	12131.32	14371.26	2999.96	350	16597.14	19438.70	4083.97
355	12125.43	14543.28	3060.59	355	16591.41	19674.06	4166.94
360	12132.18	14712.91	3121.23	360	16603.23	19906.17	4249.92
365	12149.29	14880.36	3181.93	365	16629.35	20135.35	4332.99
370	12174.45	15045.82	3242.74	370	16666.52	20361.85	4416.23
375	12205.37	15209.44	3303.69	375	16711.48	20585.86	4499.67
380	12239.75	15371.32	3364.80	380	16760.98	20807.53	4583.35
385	12275.29	15531.56	3426.09	385	16811.76	21026.96	4667.28
390	12309.71	15690.17	3487.55	390	16860.58	21244.21	4751.47
395	12340.70	15847.19	3549.18	395	16904.17	21459.28	4835.88
400	12365.96	16002.58	3610.95	400	16939.29	21672.14	4920.49
PEG10000				PEG12000			
T/K	$C^o_{p,m}$/ (J·K^{-1}·mol^{-1})	$\Delta_0^T S^o_m$/ (J·K^{-1}·mol^{-1})	$\Delta_0^T H^o_m$/ (kJ·mol^{-1})	T/K	$C^o_{p,m}$/ (J·K^{-1}·mol^{-1})	$\Delta_0^T S^o_m$/ (J·K^{-1}·mol^{-1})	$\Delta_0^T H^o_m$/ (kJ·mol^{-1})
Solid region				Solid region			
0	0	0	0	0	0	0	0
1	2.5219E−01	8.3567E−02	6.2738E−05	1	3.0276E−01	1.0026E−01	7.5281E−05
2	2.1001E+00	6.8557E−01	1.0321E−03	2	2.5317E+00	8.2471E−01	1.2420E−03
3	7.4758E+00	2.3984E+00	5.4343E−03	3	9.0614E+00	2.8959E+00	6.5661E−03
4	1.8656E+01	5.9140E+00	1.7920E−02	4	2.2735E+01	7.1700E+00	2.1747E−02
5	3.7748E+01	1.1966E+01	4.5396E−02	5	4.6209E+01	1.4564E+01	5.5319E−02
6	6.5744E+01	2.1189E+01	9.6407E−02	6	8.0726E+01	2.5875E+01	1.1788E−01
7	101.13	3.3910E+01	1.7938E−01	7	124.39	4.1510E+01	2.1986E−01
8	142.47	5.0046E+01	3.0068E−01	8	175.42	6.1369E+01	3.6915E−01
9	189.55	6.9491E+01	4.6624E−01	9	233.54	8.5320E+01	5.7307E−01
10	241.85	9.2126E+01	6.8153E−01	10	298.11	113.21	8.3839E−01
15	565.79	248.34	2.6624E+00	15	697.82	305.86	3.2812E+00
20	958.74	463.77	6.4537E+00	20	1182.11	571.52	7.9566E+00
25	1383.69	723.03	1.2303E+01	25	1705.02	891.10	1.5166E+01
30	1814.76	1013.47	2.0300E+01	30	2234.59	1248.85	2.5017E+01
35	2234.97	1324.99	3.0432E+01	35	2749.90	1632.29	3.7488E+01
40	2634.21	1649.76	4.2615E+01	40	3238.64	2031.73	5.2472E+01
45	3007.57	1981.85	5.6730E+01	45	3694.95	2439.87	6.9820E+01
50	3353.92	2316.89	7.2645E+01	50	4117.65	2851.34	8.9365E+01
55	3674.70	2651.79	9.0227E+01	55	4508.72	3262.37	110.94
60	3973.00	2984.47	109.35	60	4872.16	3670.44	134.41
65	4252.76	3313.63	129.93	65	5212.96	4074.02	159.63
70	4518.15	3638.59	151.86	70	5536.41	4472.27	186.51
75	4773.21	3959.05	175.09	75	5847.51	4864.90	214.97
80	5021.42	4275.06	199.58	80	6150.60	5252.00	244.97
85	5265.60	4586.82	225.30	85	6449.14	5633.85	276.47
90	5507.75	4894.66	252.23	90	6745.53	6010.87	309.46
95	5749.03	5198.91	280.37	95	7041.12	6383.51	343.92
100	5989.83	5499.92	309.72	100	7336.29	6752.18	379.87
110	6468.07	6093.30	372.02	110	7922.55	7478.96	456.17
120	6933.77	6676.20	439.04	120	8492.69	8192.94	538.26
130	7373.95	7248.79	510.61	130	9030.06	8894.21	625.91
140	7776.54	7810.25	586.39	140	9519.51	9581.65	718.71
150	8134.79	8359.26	665.99	150	9952.95	10253.54	816.12
160	8450.23	8894.54	748.95	160	10333.05	10908.28	917.59
170	8733.75	9415.46	834.89	170	10674.41	11545.10	1022.65
180	9004.52	9922.34	923.58	180	11002.04	12164.50	1131.03
190	9287.02	10416.65	1015.02	190	11347.38	12768.45	1242.75
200	9606.34	10900.92	1109.44	200	11742.20	13360.26	1358.14
210	9982.71	11378.46	1207.33	210	12327.75	13947.85	1478.60
220	10558.87	11856.30	1310.07	220	13117.04	14538.52	1605.60
230	11168.49	12339.09	1418.70	230	13982.58	15141.12	1741.19
240	11727.04	12826.54	1533.26	240	14650.76	15751.11	1884.54
250	12205.91	13315.15	1652.97	250	15191.35	16360.20	2033.77
260	12685.17	13803.04	1777.38	260	15801.91	16967.49	2188.63
270	13248.21	14292.01	1906.96	270	16525.58	17577.17	2350.20
273.15	13446.61	14446.82	1949.00	273.15	16767.32	17770.25	2402.63

(*continued on next page*)

Table 7 (*continued*)

PEG10000				PEG12000			
T/K	$C^o_{p,m}$/ (J·K^{-1}·mol^{-1})	$\Delta_0^T S^o_m$/ (J·K^{-1}·mol^{-1})	$\Delta_0^T H^o_m$/ (kJ·mol^{-1})	T/K	$C^o_{p,m}$/ (J·K^{-1}·mol^{-1})	$\Delta_0^T S^o_m$/ (J·K^{-1}·mol^{-1})	$\Delta_0^T H^o_m$/ (kJ·mol^{-1})
280	13907.91	14785.48	2042.67	280	17318.34	18192.25	2519.35
290	14662.10	15286.33	2185.42	290	18276.42	18815.92	2697.10
298.15	15417.04	15702.69	2307.87	298.15	19291.06	19335.94	2850.04
300	15616.85	15798.67	2336.57	300	19552.02	19456.07	2885.96
305	16212.33	16061.61	2416.11	305	20322.37	19785.44	2985.60
310	16841.79	16330.37	2498.76	310	21298.40	20123.34	3089.51
Melting region				Melting region			
315	17652.76	16606.28	2584.98	315	22617.99	20473.40	3198.91
320	19091.34	16893.62	2676.22	320	28683.81	20863.55	3322.82
325	38040.02	17275.34	2799.44	325	50575.97	21459.28	3515.08
330	95180.15	18097.99	3069.14	330	148247.32	22748.90	3938.01
335	313003.30	21316.26	4141.13	335	210622.67	26818.43	5292.14
340	23081.22	23036.25	4719.69	340	24214.14	27699.94	5588.74
345	20021.13	23336.48	4822.50	345	23870.43	28049.72	5708.54
Liquid region				Liquid region			
350	19946.59	23623.65	4922.29	350	23814.55	28392.42	5827.62
355	19975.17	23906.79	5022.09	355	23844.88	28730.42	5946.77
360	20006.50	24186.38	5122.05	360	23880.53	29064.17	6066.08
365	20040.59	24462.57	5222.16	365	23921.49	29393.83	6185.58
370	20077.42	24735.48	5322.46	370	23967.78	29719.61	6305.30
375	20117.01	25005.24	5422.94	375	24019.39	30041.67	6425.27
380	20159.35	25271.97	5523.63	380	24076.31	30360.18	6545.50
385	20204.44	25535.79	5624.54	385	24138.56	30675.31	6666.04
390	20252.28	25796.80	5725.68	390	24206.12	30987.21	6786.90
395	20302.87	26055.11	5827.07	395	24279.01	31296.03	6908.11
400	20356.21	26310.83	5928.71	400	24357.21	31601.91	7029.70

PEG20000							
T/K	$C^o_{p,m}$/ (J·K^{-1}·mol^{-1})	$\Delta_0^T S^o_m$/ (J·K^{-1}·mol^{-1})	$\Delta_0^T H^o_m$/ (kJ·mol^{-1})	T/K	$C^o_{p,m}$/ (J·K^{-1}·mol^{-1})	$\Delta_0^T S^o_m$/ (J·K^{-1}·mol^{-1})	$\Delta_0^T H^o_m$/ (kJ·mol^{-1})
Solid region				180	17755.07	19575.43	1821.77
0	0	0	0	190	18317.87	20550.24	2002.09
1	4.8130E−01	1.5937E−01	1.1966E−04	200	18956.64	21505.65	2188.38
2	4.0284E+00	1.3116E+00	1.9755E−03	210	20116.20	22457.47	2383.51
3	1.4436E+01	4.6095E+00	1.0453E−02	220	21806.64	23430.80	2592.81
4	3.6267E+01	1.1424E+01	3.4657E−02	230	23433.49	24437.71	2819.39
5	7.3806E+01	2.3227E+01	8.8248E−02	240	24531.74	25459.94	3059.61
6	129.08	4.1303E+01	1.8823E−01	250	25399.67	26478.87	3309.25
7	198.90	6.6304E+01	3.5131E−01	260	26442.30	27494.56	3568.25
8	280.52	9.8060E+01	5.9003E−01	270	27656.00	28515.03	3838.68
9	373.48	136.36	9.1613E−01	273.15	28046.05	28838.08	3926.41
10	476.77	180.97	1.3404E+00	280	28920.72	29543.39	4121.48
15	1116.60	489.15	5.2484E+00	290	30483.71	30584.01	4418.07
20	1892.75	914.39	1.2732E+01	298.15	32191.58	31451.57	4673.22
25	2731.93	1426.26	2.4280E+01	300	32625.90	31652.03	4733.17
30	3583.00	1999.69	4.0070E+01	305	33883.97	32201.48	4899.38
35	4412.39	2614.73	6.0073E+01	310	35489.96	32764.60	5072.55
40	5200.19	3255.89	8.4124E+01	Melting region			
45	5936.75	3911.43	111.99	315	37566.43	33347.43	5254.70
50	6619.87	4572.75	143.40	320	43890.47	33974.29	5453.76
55	7252.48	5233.74	178.10	325	73665.02	34855.90	5738.27
60	7840.70	5890.30	215.85	330	154544.25	36391.17	6241.54
65	8392.34	6539.89	256.45	335	652529.17	41842.76	8057.54
70	8915.69	7181.13	299.73	340	52845.11	46254.02	9542.00
75	9418.68	7813.50	345.57	345	40861.28	46887.47	9758.90
80	9908.22	8437.05	393.89	350	40556.35	47472.71	9962.26
85	10389.83	9052.21	444.64	Liquid region			
90	10867.42	9659.61	497.79	355	40574.29	48047.63	10164.92
95	11343.26	10259.93	553.31	360	40682.83	48615.87	10368.07
100	11818.06	10853.84	611.22	365	40783.76	49177.73	10571.73
110	12760.64	12024.54	734.12	370	40877.09	49733.26	10775.89
120	13677.77	13174.46	866.35	375	40962.81	50282.54	10980.49
130	14543.84	14303.89	1007.51	380	41040.94	50825.62	11185.51
140	15335.26	15411.19	1156.97	385	41111.46	51362.58	11390.89
150	16039.23	16493.73	1313.92	390	41174.37	51893.47	11596.61
160	16659.55	17549.08	1477.48	395	41229.69	52418.35	11802.62
170	17218.58	18576.06	1646.90	400	41277.40	52937.28	12008.89

[a] All calculated thermodynamic values have estimated standard uncertainties of about 0.05·X below 20 K, 0.02·X from (20 to 300) K, and 0.05·X above 300 K for PEG1500, 2000, 4000, 6000, 8000, 10,000 and 20000; about 0.1·X below 20 K, 0.02·X from (20 to 300) K, and 0.07·X above 300 K for PEG1000; and about 0.05·X below 20 K, 0.02·X from (20 to 300) K, and 0.08·X above 300 K for PEG12000; where X represents the thermodynamic property.

kJ·mol^{-1} for PEG8000; (15417.04 ± 308.34) J·K^{-1}·mol^{-1}, (15702.69 ± 314.06) J·K^{-1}·mol^{-1} and (2307.87 ± 46.16) kJ·mol^{-1} for PEG10000; (19291.06 ± 385.82) J·K^{-1}·mol^{-1}, (19335.94 ± 386.72) J·K^{-1}·mol^{-1} and (2850.04 ± 57.00) kJ·mol^{-1} for PEG12000; and (32191.58 ± 643.84) J·K^{-1}·mol^{-1}, (31451.57 ± 629.04) J·K^{-1}·mol^{-1} and (4673.22 ± 93.46) kJ·mol^{-1} for PEG20000, respectively.

$$\Delta H_0^T = \int_0^T C_{p,m} dT \tag{3}$$

$$\Delta S_0^T = \int_0^T (C_{p,m}/T) dT \tag{4}$$

4. Conclusions

In this work, the thermal stability, thermal conductivity and phase change properties of the PEG samples with molar mass of 1000, 1500, 2000, 4000, 6000, 8000, 10000, 12,000 and 20,000 were studied using different thermal analysis method, and these thermal properties obtained in this work were compared with the previous results. Most importantly, the heat capacities of these PEG samples were measured using a combination of PPMS and DSC calorimetric methods in the temperature range from (1.9 to 400) K for the first time, and the corresponding thermodynamic functions of these PEG samples were calculated based on the heat capacity curve fitting. The standard molar heat capacity ($C^o_{p,m}$), entropy (S^o_m) and enthalpy (H^o_m) at 298.15 K and 0.1 MPa have been determined to be (5767.85 ± 115.36) J·K^{-1}·mol^{-1}, (1753.06 ± 35.06) J·K^{-1}·mol^{-1} and (276.56 ± 5.54) kJ·mol^{-1} for PEG1000; (2992.37 ± 59.44) J·K^{-1}·mol^{-1}, (2735.50 ± 54.75) J·K^{-1}·mol^{-1} and (436.54 ± 8.74) kJ·mol^{-1} for PEG1500; (3612.71 ± 72.26) J·K^{-1}·mol^{-1}, (3195.74 ± 63.92) J·K^{-1}·mol^{-1} and (478.75 ± 9.58) kJ·mol^{-1} for PEG2000; (6564.54 ± 131.3) J·K^{-1}·mol^{-1}, (6306.98 ± 126.08) J·K^{-1}·mol^{-1} and (930.98 ± 18.62) kJ·mol^{-1} for PEG4000; (9633.64 ± 192.68) J·K^{-1}·mol^{-1}, (9488.32 ± 189.76) J·K^{-1}·mol^{-1} and (1394.12 ± 27.88) kJ·mol^{-1} for PEG6000; (13281.44 ± 265.62) J·K^{-1}·mol^{-1}, (12726.68 ± 254.54) J·K^{-1}·mol^{-1} and (1879.33 ± 37.58) kJ·mol^{-1} for PEG8000; (15417.04 ± 308.34) J·K^{-1}·mol^{-1}, (15702.69 ± 314.06) J·K^{-1}·mol^{-1} and (2307.87 ± 46.16) kJ·mol^{-1} for PEG10000; (19291.06 ± 385.82) J·K^{-1}·mol^{-1}, (19335.94 ± 386.72) J·K^{-1}·mol^{-1} and (2850.04 ± 57.00) kJ·mol^{-1} for PEG12000; and (32191.58 ± 643.84) J·K^{-1}·mol^{-1}, (31451.57 ± 629.04) J·K^{-1}·mol^{-1} and (4673.22 ± 93.46) kJ·mol^{-1} for PEG20000, respectively. The thermal properties and thermodynamic data obtained in this work would be technically necessary and important for theoretically studying and actually using PEG as phase change materials for thermal energy applications.

Acknowledgements

The authors gratefully acknowledge the National Natural Science Foundation of China under grant 21473198, Liaoning Provincial Natural Science Foundation of China under grant 201602741. Q. Shi would like to thank Hundred-Talent Program founded by Chinese Academy of Sciences.

Appendix A. Supplementary data

Supplementary data associated with this article can be found, in the online version, at https://doi.org/10.1016/j.jct.2018.08.031.

References

[1] G. Faninger, Thermal Energy Storage, In: Faculty for Interdisciplinary Research and Continuing Education, IFF-University of Klagenfurt, Austria, 2004.
[2] A. Sharma, V.V. Tyagi, C.R. Chen, D. Buddhi, Review on thermal energy storage with phase change materials and applications, Renew. Sustain. Energy Rev. 13 (2009) 318–345.
[3] D.C. Hyun, N.S. Levinson, U. Jeong, Y. Xia, Emerging applications of phase-change materials (PCMs): teaching an old dog new tricks, Angew Chem. Int. Ed. 53 (2014) 3780–3795.
[4] S. Sundararajan, A.B. Samui, P.S. Kulkarni, Versatility of polyethylene glycol (PEG) in designing solid-solid phase change materials (PCMs) for thermal management and their application to innovative technologies, J. Mater. Chem. A 5 (2017) 18379–18396.
[5] A. Kuru, S.A. Aksoy, Cellulose–PEG grafts from cotton waste in thermo-regulating textiles, Text. Res. J. 84 (2014) 337–346.
[6] X.W. Wang, H.W. Hu, Z.Y. Yang, L. He, Y.Y. Kong, B. Fei, J.H. Xin, Smart hydrogel-functionalized textile system with moisture management property for skin application, Smart Mater. Struct. 23 (2014) 125027.
[7] W. Wu, X. Huang, K. Li, R. Yao, R. Chen, R. Zou, A functional form-sTable phase change composite with high efficiency electro-to-thermal energy conversion, Appl. Energy 190 (2017) 474–480.
[8] Y.M. Wang, B.T. Tang, S.F. Zhang, Single-walled carbon nanotube/phase change material composites: sunlight-driven, reversible, form-stable phase transitions for solar thermal energy storage, Adv. Funct. Mater. 23 (2013) 4354–4360.
[9] Y. Jiang, Z. Wang, M. Shang, Z. Zhang, S. Zhang, Heat collection and supply of interconnected netlike graphene/polyethyleneglycol composites for thermoelectric devices, Nanoscale 7 (2015) 10950–10953.
[10] H. Kim, D. Lee, J. Kim, T. Kim, W.J. Kim, Photothermally triggered cytosolic drug delivery via endosome disruption using a functionalized reduced graphene oxide, ACS Nano 7 (2013) 6735–6746.
[11] S. Sundararajan, A.B. Samui, P.S. Kulkarni, Interpenetrating phase change polymer networks based on crosslinked polyethylene glycol and poly (hydroxylethyl methacrylate), Sol. Energy Mater. Sol. Cells 149 (2016) 266–274.
[12] J. Yang, E. Zhang, X. Li, Y. Zhang, J. Qu, Z. Yu, Cellulose/graphene aerogel supported phase change composites with high thermal conductivity and good shape stability for thermal energy storage, Carbon 98 (2016) 50–57.
[13] Y. Zhou, D.K. Sheng, X.D. Liu, C.H. Lin, F.C. Ji, L. Dong, S.B. Xu, Y.M. Yang, Synthesis and properties of crosslinking halloysite nanotubes/polyurethane based solid-solid phase change materials, Sol. Energy Mater. Sol. Cells 174 (2018) 84–93.
[14] J.J. Wang, M. Yang, Y.F. Lu, Z.K. Jin, L. Tan, H.Y. Gao, S. Fan, W.J. Dong, G. Wang, Surface functionalization engineering driven crystallization behavior of polyethylene glycol confined in mesoporous silica for shape-stabilized phase change materials, Nano Energy 19 (2016) 78–87.
[15] R.X. Dai, S.H. Zhang, N. Yin, Z.C. Tan, Q. Shi, Low-temperature heat capacity and standard thermodynamic functions of β-D-(-)-arabinose ($C_5H_{10}O_5$), J. Chem. Thermodyn. 92 (2016) 60–65.
[16] Q. Shi, J. Boerio-Goates, B.F. Woodfield, An improved technique for accurate heat capacity measurements on powdered samples using a commercial relaxation calorimeter, J. Chem. Thermodyn. 43 (2011) 1263–1269.
[17] Q. Shi, L.S. Claine, B.G. Juliana, B.F. Woodfield, Accurate heat capacity measurements on powdered samples using a quantum design physical property measurement system, J. Chem. Thermodyn. 42 (2010) 1107–1109.
[18] K. Pielichowski, K. Fleituch, Differential scanning calorimetry studies on poly (ethylene glycol) with different molar massfor thermal energy storage materials, Polym. Adv. Technol. 13 (2002) 690–696.
[19] B. Ellis, R. Smith, Polymers: A property Database, second ed., CSC Press, Tayor &Francis Group, USA, 2009.
[20] S. Karaman, A. Karaipekli, A. Sarı, A. Bicer, Polyethyleneglycol (PEG)/diatomite composite as a novel form-STable phase change material for thermal energy storage, Sol. Energy Mater. Sol. Cells 95 (2011) 1647–1653.
[21] J. Tang, M. Yang, W. Dong, M. Yang, H. Zhang, S. Fan, J. Wang, L. Tan, G. Wang, Highly porous carbons derived from MOFs for shape-stabilized phase change materials with high storage capacity and thermal conductivity, RSC Adv. 6 (2016) 40106–40114.
[22] B.T. Tang, C. Wu, M.G. Qiu, X.W. Zhang, S.F. Zhang, PEG/SiO_2-Al_2O_3 hybrid form-STable phase change materials with enhanced thermal conductivity, Mater. Chem. Phy. 144 (2014) 162–167.
[23] J. Yang, L.S. Tang, R.Y. Bao, L. Bai, Z.Y. Liu, W. Yang, B.H. Xie, M.B. Yang, An ice-templated assembly strategy to construct graphene oxide/boron nitride hybrid porous scaffolds in phase change materials with enhanced thermal conductivity and shape stability for light–thermal–electric energy conversion, J. Mater. Chem. A 4 (2016) 18841–18851.
[24] H. Li, G.Y. Fang, Experimental investigation on the characteristics of polyethylene glycol/cement composites as thermal energy storage materials, Chem. Eng. Technol. 33 (2010) 1650–1654.
[25] L.L. Feng, W. Zhao, J. Zheng, S. Frisco, P. Song, X.G. Li, The shape-stabilized phase change materials composed of polyethylene glycol and various mesoporous matrices (AC, SBA-15 and MCM-41), Sol. Energy Mater. Sol. Cells 95 (2011) 3550–3556.
[26] P.M. Pavel, M. Constantinescu, E.M. Anghel, M. Olteanu, Solidification of a PEG 1500-epoxy nanocomposite around a horizontal pipe, Appl. Energy 89 (2012) 482–489.

[27] Y.T. Fang, H.Y. Kang, W.L. Wang, H. Liu, X.N. Gao, Study on polyethylene glycol/epoxy resin composite as a form-STable phase change material, Energy Coners. Manage. 51 (2010) 2757–2761.
[28] Y. Deng, J.H. Li, T.T. Qian, W.M. Guan, Y.L. Li, X.P. Yin, Thermal conductivity enhancement of polyethylene glycol/expanded vermiculite shape-stabilized composite phase change materials with silver nanowire for thermal energy storage, Chem. Eng. J. 295 (2016) 427–435.
[29] T.T. Qian, J.H. Li, X. Min, W.M. Guan, Y. Deng, L. Ning, Enhanced thermal conductivity of PEG/diatomite shape-stabilized phase change materials with Ag nanoparticles for thermal energy storage, J. Mater. Chem. A 3 (2015) 8526–8536.
[30] P. Xi, Y.Q. Duan, P.F. Fei, L. Xia, R. Liu, B.W. Cheng, Synthesis and thermal energy storage properties of the polyurethane solid-solid phase change materials with a novel tetrahydroxy compound, Eur. Polym. J. 48 (2012) 1295–1303.
[31] J. Yang, L.S. Tang, R.Y. Bao, L. Bai, Z.Y. Liu, B.H. Xie, M.B. Yang, W. Yang, Hybrid network structure of boron nitride and graphene oxide in shape-stabilized composite phase change materials with enhanced thermal conductivity and light-to-electric energy conversion capability, Sol. Energy Mater. Sol. Cells 174 (2018) 56–64.
[32] C. Alkan, E. Gunther, S. Hiebler, O. Ensari, D. Kahraman, Polyurethanes as solid-solid phase change materials for thermal energy storage, Sol. Energy 86 (2012) 1761–1769.
[33] A. Sari, C. Alkan, A. Karaipekli, O. Uzun, Poly(ethylene glycol)/Poly(methyl methacrylate) blends as Novel Form-STable phase-change materials for thermal energy storage, J. Appl. Polym. Sci. 116 (2010) 929–933.
[34] R. Jia, K. Sun, R. Li, Y. Zhang, W. Wang, H. Yin, D. Fang, Q. Shi, Z.C. Tan, Heat capacities of some sugar alcohols as phase change materials for thermal energy storage applications, J. Chem. Thermodyn. 115 (2017) 233–248.

JCT 2018-305